© Med Sci Monit, 2012; 18(11): CR635-642
PMID: 23111738

WWW.MEDSCIMONIT.COM
Clinical Research

CR

Received: 2012.03.21
Accepted: 2012.04.16
Published: 2012.11.01

Ultrasound elastography as a tool for imaging guidance during prostatectomy: Initial experience

Authors' Contribution:
A Study Design
B Data Collection
C Statistical Analysis
D Data Interpretation
E Manuscript Preparation
F Literature Search
G Funds Collection

Ioana Nicolaescu Fleming[1ABCDEF], Carmen Kut[1,2ABCDF], Katarzyna J. Macura[2ABDEG], Li-Ming Su[3ABD], Hassan Rivaz[1ABC], Caitlin Schneider[1ABC], Ulrike Hamper[2D], Tamara Lotan[2C], Russ Taylor[1ADG], Gregory Hager[1ADG], Emad Boctor[1,2ABDEG]

[1] Johns Hopkins University, Baltimore, MD, U.S.A.
[2] Johns Hopkins University School of Medicine, Baltimore, MD, U.S.A.
[3] Department of Urology, University of Florida College of Medicine, Gainesville, FL, U.S.A.

Source of support: This work was supported by: NSF ERC grant EEC9731748, NIH grant 2R42RR019159, and NIH/NCI grant P50CA103175

Summary

Background: During laparoscopic or robotic assisted laparoscopic prostatectomy, the surgeon lacks tactile feedback which can help him tailor the size of the excision. Ultrasound elastography (USE) is an emerging imaging technology which maps the stiffness of tissue. In the paper we are evaluating USE as a palpation equivalent tool for intraoperative image guided robotic assisted laparoscopic prostatectomy.

Material/Methods: Two studies were performed: 1) A laparoscopic ultrasound probe was used in a comparative study of manual palpation versus USE in detecting tumor surrogates in synthetic and *ex-vivo* tissue phantoms; N=25 participants (students) were asked to provide the presence, size and depth of these simulated lesions, and 2) A standard ultrasound probe was used for the evaluation of USE on *ex-vivo* human prostate specimens (N=10 lesions in N=6 specimens) to differentiate hard versus soft lesions with pathology correlation. Results were validated by pathology findings, and also by *in-vivo* and *ex-vivo* MR imaging correlation.

Results: In the comparative study, USE displayed higher accuracy and specificity in tumor detection (sensitivity=84%, specificity=74%). Tumor diameters and depths were better estimated using USE versus with manual palpation. USE also proved consistent in identification of lesions in *ex-vivo* prostate specimens; hard and soft, malignant and benign, central and peripheral.

Conclusions: USE is a strong candidate for assisting surgeons by providing palpation equivalent evaluation of the tumor location, boundaries and extra-capsular extension. The results encourage us to pursue further testing in the robotic laparoscopic environment.

key words: **prostatectomy • laparoscopy • robotics • ultrasonography • elastography**

Full-text PDF: http://www.medscimonit.com/fulltxt.php?ICID=883540

Word count: 3631
Tables: 2
Figures: 7
References: 31

Author's address: Ioana Fleming, 112 Hackerman Hall, 3400 N. Charles Street, Baltimore, MD 21218, U.S.A., e-mail: inicola1@jhu.edu

Background

Prostate cancer is the second leading cause of cancer death and the most common cancer detected in men in the United States. An estimated 217,730 new cases of prostate cancer were diagnosed in the United States, and approximately 32,050 men died of prostate cancer during 2010 [1]. Radical Prostatectomy (RP) aims for complete cancer resection and has been shown to improve cancer survival [2]. Robotic-assisted laparoscopic prostatectomy (RALP) has recently emerged as an alternative to open and laparoscopic procedures. The daVinci Surgical System (Intuitive Surgical, Sunnyvale, CA) provides 3-D visualization, higher magnification, hand tremor elimination and refined dexterity by incorporating wristed instrumentation. From 250 robotic cases in the beginning (2001), the number has reached 73,000 in 2009 (86% of the 85,000 American men who had prostate cancer surgery) [3,4].

Initial experiences with the daVinci surgical system have been positive: short learning curve, limited blood loss, less post-operative pain, favorable complication rates, and short hospital stay [3–10]. Despite fewer perioperative complications and shorter hospital stay, a recent paper found patients were three times more likely to require salvage therapy [11]. One theoretical disadvantage with regards to robotic surgery is the lack of tactile feedback. In open RPs, the surgeon uses his fingers to feel the periphery of the prostate gland [12]. Without tactile feedback, a robotic surgeon is unable to appreciate differences in tissue texture or firmness and therefore may not be able to tailor precisely the extent of tissue excision around the prostate gland in efforts to eradicate all cancerous tissue. Inadvertently leaving residual cancer cells behind, called a positive surgical margin (PSM), is highly associated with cancer recurrence. PSM rates were initially higher in RALP than in the open procedure, but they have been shown to decrease with surgeon's experience and improved technique [9,11].

As manual palpation helps guide the surgeon in the open procedure, an equivalent real-time guiding tool is needed for robotic prostatectomy. Imaging modalities like MRI or CT are not feasible intraoperatively, nor do they possess the sensitivity or specificity for accurate detection and localization of prostate cancer. Transrectal ultrasound (TRUS) is routinely used in diagnosis, in conjunction with digital rectal examination (DRE) and biopsies [13]. One center used TRUS for real-time monitoring and guidance during Laparoscopic RP and reported technical feasibility and enhanced precision by decreased PSM rates [14,15]. TRUS was capable of imaging a substantial percent of nonpalpable prostate cancers. The authors recognized however, the limitations of TRUS guidance; it requires considerable prior expertise and tends to identify primarily hypoechoic lesions, which were just 47% of the cancer nodules studied [15]. Today's prostate cancer patients are more likely to present with echogenic or isoechoic lesions because aggressive screening techniques lead to a shift toward smaller, early-stage cancers [16,17]; classic B-mode gray-scale ultrasound alone cannot identify these lesions.

Ultrasound (US) Elastography (USE) is emerging as a valuable tool in the field of imaging. Elastography is a qualitative technique based on the principle that tissue compression produces strain (displacement) within that tissue; strain is smaller in harder, stiffer tissue than in softer, more compliant tissue [18]. Analyzing the ultrasound raw radio frequency signal results in a strain map, commonly called *elastogram*, where harder tissue is darker than surrounding soft tissue. Cancers tend to present as hard lesions due to increased cellularity [18]. Echogenicity and stiffness of tissue are generally uncorrelated; USE can identify hypoechoic lesions, but also echogenic or isoechoic cancers that classic gray-scale ultrasonography cannot. Elastography through the transrectal approach has already been proven feasible in guiding biopsies of the prostate [19–22]. Integrating USE technology with a laparoscopic ultrasound probe will give robotic and laparoscopic surgeons an important image-guidance tool, which until this point does not exist [23–25].

This paper describes two experiments and results of an ongoing study evaluating the diagnostic accuracy and efficacy of using USE to identify the cancerous nodules in the prostate gland. The aim of the first study was to compare the ability of subjects to detect hard tissue (tumor surrogates) in synthetic and *ex-vivo* phantoms. We attempted to mimic an OR setting of open *vs.* robotic procedures, by asking the subjects to identify properties of the tissue using manual palpation in one arm, versus using ultrasound elastograms in the other arm. The elastograms were obtained with a laparoscopic ultrasound probe. In the second study, human *ex-vivo* prostatectomy specimens where used to assess the accuracy of USE in the identification and characterization of hard cancerous nodules. We compared the elastogram results with histopathology maps (the gold standard) and also to pre- and post-operative MR scans of the prostate gland in order to assess and co-localize anatomically USE with the reference histopathology and MR scans.

Material and Methods

Comparative study for USE *vs.* manual palpation in tumor detection

Institutional Review Board approval was obtained for the comparative study. We recruited N=25 local students to asses human ability to feel hard lesions through palpation, versus elastography's ability to distinguish the same lesions. Our decision to use local students instead of seasoned surgeons stemmed from the rationale that all humans are born with the sense of touch and thus have the innate sensory ability to palpate; we were also able to recruit more subjects in order to assess inter-observer variability. Participants were asked to identify lesions present in both synthetic and *ex-vivo* phantoms. The subjects evaluated the phantoms using manual palpation and ultrasound based elastograms. The hypothesis of the study was that subjects could identify lesions easier on the elastograms versus using manual palpation. Seven synthetic and four *ex-vivo* tissue phantoms were created. The phantoms mimicked the mechanical properties of prostate tissue and the acoustic scattering properties of human tissue. *Synthetic phantoms* exhibited deeper spherical hard lesions, consistent with deeper prostatic cancerous nodules, while *Ex-vivo phantoms* had superficial, free-form ablated lesions, more consistent with extra-capsular cancer extension.

Synthetic phantoms (3×2×2 inches) were made from Liquid Plastic (M-F Manufacturing Co., Inc., Haltom City, TX) and

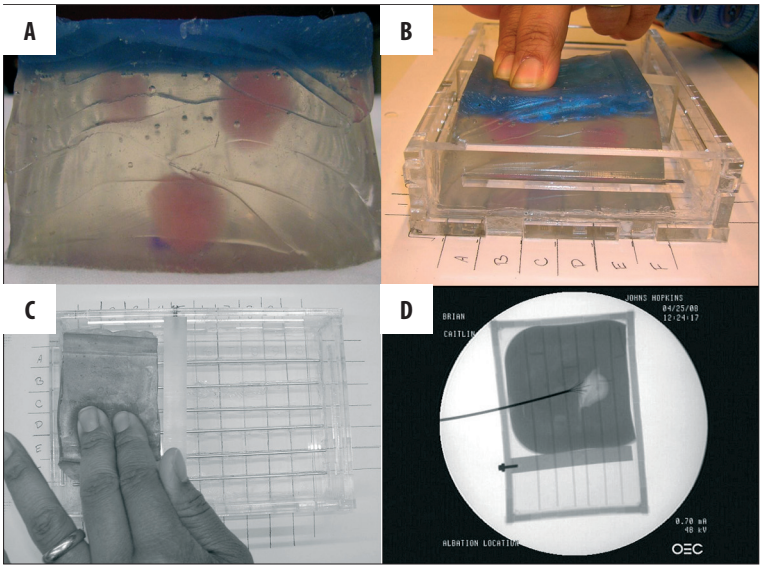

Figure 1. Synthetic phantoms: (**A**) lesions are visible from the side (pink) and the top is opaque (dark blue); (**B,C**) inside the grid calibration container; (**D**) X-ray of *ex-vivo* chicken phantom. Ablation probe, tines and the grid calibration container are visible.

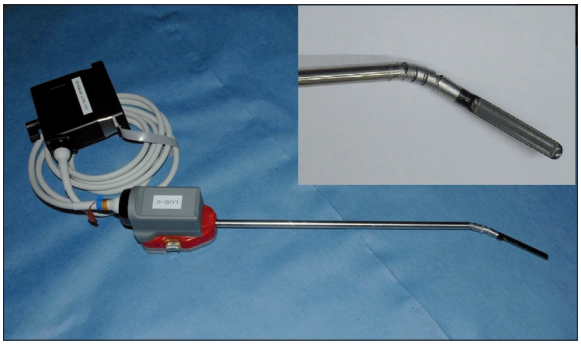

Figure 2. Laparoscopic ultrasound probe; close-up view of the probe's head (insert). Prototype courtesy of Intuitive Surgical.

glass micro-beads. The micro-beads were used as a scattering material. They were added to the plastic mix in an 1% concentration to mimic the acoustic scattering properties of human tissue; both the lesions and the rest of the phantom appeared isoechoic under B-mode ultrasound. Lesions were created by varying the mixing ratios of liquid plastic types; the ratio between 4116S Plastic Softener or 7116 Plastic Hardener and 8116 Super-Soft Plastic determined the final density and the elastic modulus of the lesions and the background [26]. Each phantom contained 0-3 harder spherical lesions (1-2 cm diameter) colored pink for ground truth identification (Figure 1A). The exposed top surface was colored opaque blue, to prevent the subjects from visually identifying the lesions (Figure 1A). The *synthetic phantoms* were sliced and sectioned at study end, following axial planes parallel with the ultrasound scanning plane. The depth of each lesion was measured as the distance between the surface of the phantom and the top of the lesion itself. The final depth of lesions for these 7 (seven) phantoms was measured to be between 7 and 25 mm.

Ex-vivo phantoms were constructed from raw chicken breast tissue. Hard lesions of various diameters were created using radio frequency (RF) ablation, at an average temperature of 95 degrees Fahrenheit for 20 minutes. This formed a hard spherical lesion at a depth of 1–6 mm below the surface, which allowed for possible palpation but not the visual localization of lesions. Before ablation, each tissue was placed in a small plastic container and surrounded by 150 Bloom porcine gelatin (Bloom represents an unit of measure for rigidity of gelatin). X-ray axial scans (projection plane parallel with the ultrasound scanning plane) were used to localize and measure the lesions (Figure 1D). The tissue phantoms were sliced on the same axial plane at study end to determine the depth and extent of the ablated areas. The depth of each lesion was measured as the distance between the surface of the phantom and the top of the lesion itself. For *ex-vivo* lesions, the final depth of lesions was measured to be less than 7 mm.

Hardware and software specification

For the comparative study, a laparoscopic ultrasound probe was used, fitted with a transducer (Gore Tetrad, Englewood, CO) with a center frequency of 7.5 MHz, and 128 elements (Figure 2) [23–25]. Ultrasound raw radio-frequency data was acquired using an Ultrasonix US scanner (Ultrasonix Medical Corporation, Richmond, BC, Canada). Due to the relative inexperience of our subjects, it was not possible to have the subjects perform real-time elastography. Thus, to maintain consistent image quality and to minimize user dependence, elastography images were obtained in a standardized manner by one of our researchers, prior to the evaluation. Elastograms were generated using the corresponding radio frequency data and our dynamic programming (DP) elastography algorithm [27,28].

During the study, each subject reviewed 3–4 phantoms, each placed in a self-designed calibration container, which consisted of a 5-by-5 grid, 0.5 inches apart, labeled with numbers and letters along the two axis (Figure 1B, C). Subjects were asked to identify by manual palpation the location based on the provided grid (i.e. B4 or A3), and also the diameter and depth of each lesion using 0.5 inches as the unit of reference. For the USE arm of the study, the subjects first underwent an USE training session, where they were explained the concept and shown sample elastograms. They were then presented with 3–4 elastograms of the phantoms and they were asked to provide the presence, size and

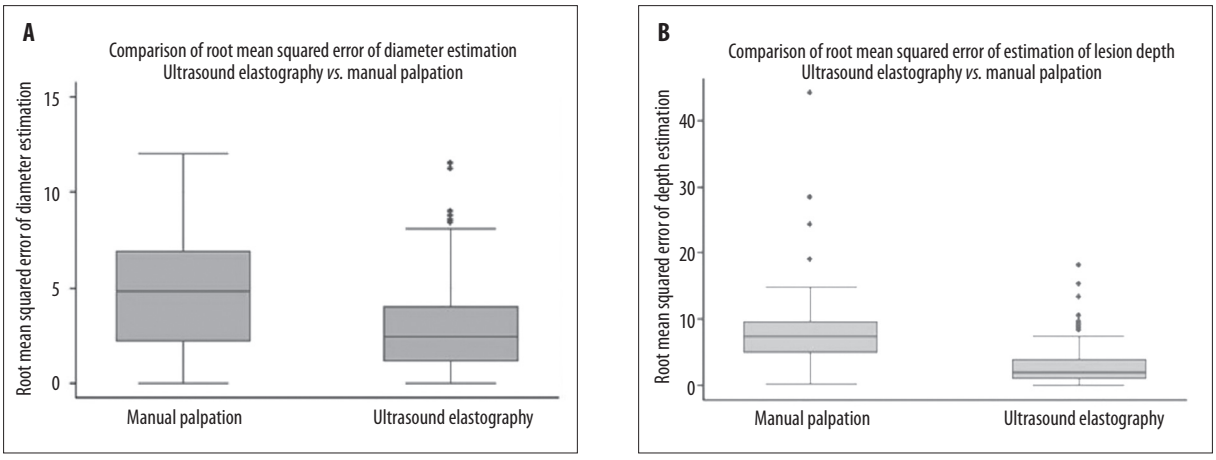

Figure 3. Synthetic phantom study results: Box-and-whisker plots for lesion diameter (**A**) and depth from surface (**B**).

depth of lesions given the scale of the images. The order in which the subjects completed the USE and manual palpation tasks was randomized.

Accuracy was determined descriptively using box and whiskers plots (Figure 3A,B), sensitivity and specificity calculations, and root mean squared error of estimation (RMSE) obtained from subtracting the estimated value of the measured parameter (diameter, depth) from the ground truth value determined from direct measurement. STATA 9 (StataCorp LP, College Station, TX) was used to perform the statistical analysis, which consisted of Student's t-test for comparison between the means of the RMSE of both diameter and depth as estimated via manual palpation versus USE. The p-values reported were generated by t-test calculations assuming unequal variances for a two-tailed test where p=0.05.

Ex-vivo human prostate study for tumor detection

Prostate cancer patients, candidates for prostatectomy, were prospectively enrolled in our study, following an informed consent approved by the Institutional Review Board. The objective of the study was to evaluate the efficacy of using elastography to identify and precisely localize hard nodules such as seen with prostate cancer just beneath the surface of the prostate gland in the peripheral zone. In this area, cancerous lesions are at most risk of invasion beyond the confines of the prostate gland and also more likely to be cut across by a well meaning surgeon. We recruited patients who underwent both open and assisted prostatectomies given that the process of removing the gland was not a focus of our study. Patients underwent multiple radiological procedures. 1) Pre-operative 3 Tesla MRI of the pelvis was performed right before the surgery procedure. 2) Post-operative ultra high-resolution MRI at 9.4 Tesla was performed on the excised prostate specimen to correlate the results to *in-vivo* pre-operative imaging. 3) USE was then performed on the prostate specimen by an experienced radiologist blinded to the surgeon's findings and to the pre-operative pathology report. The collected radio-frequency (RF) data was used offline to recreate classic B-mode grey-scale images, and also to compute elastograms showing the stiffness of the tissue scanned [27,28].

Pre-operative and post-operative MR scans were used for anatomical correlation with the computed elastograms. For

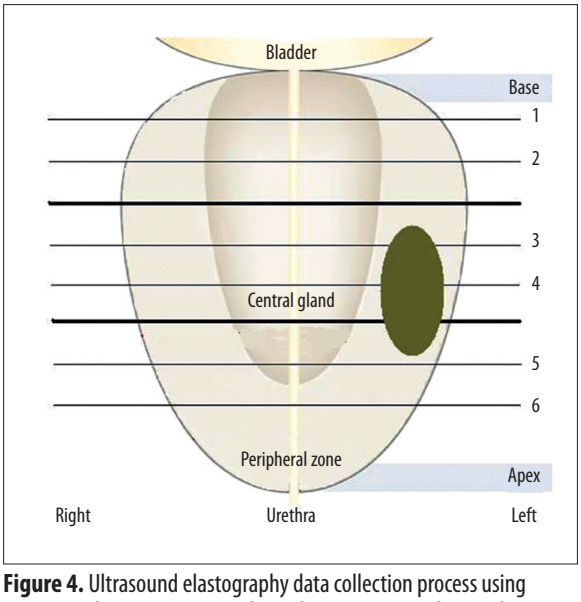

Figure 4. Ultrasound elastography data collection process using the sextant approach; RF data was acquired in axial planes (1–6) from the gland's base towards the apex. For illustration purposes, a lesion is outlined in the left mid section, peripheral zone of the specimen, similar with the case of specimen #3.

USE, the prostate specimens were placed in prone position on a surgical table. USE scans were performed in a systematic sextant approach, similar to that used for image guided biopsies. RF data was acquired in axial planes (from gland's base, through mid gland, to apex) on the left and right side of the gland (Figure 4). The sextant approach was necessary to ensure that the scans were in the same plane with the histopathology diagrams (axial) which constituted the gold standard for comparison. USE coronal scans from the left to the right of the gland were also performed; these scans were in alignment with the MR coronal scans.

Hardware and software specification

For the second study, USE acquisition was conducted using a Siemens Antares US scanner (Siemens Medical Solutions USA, Inc. Ultrasound Division, Issaquah, WA) with an

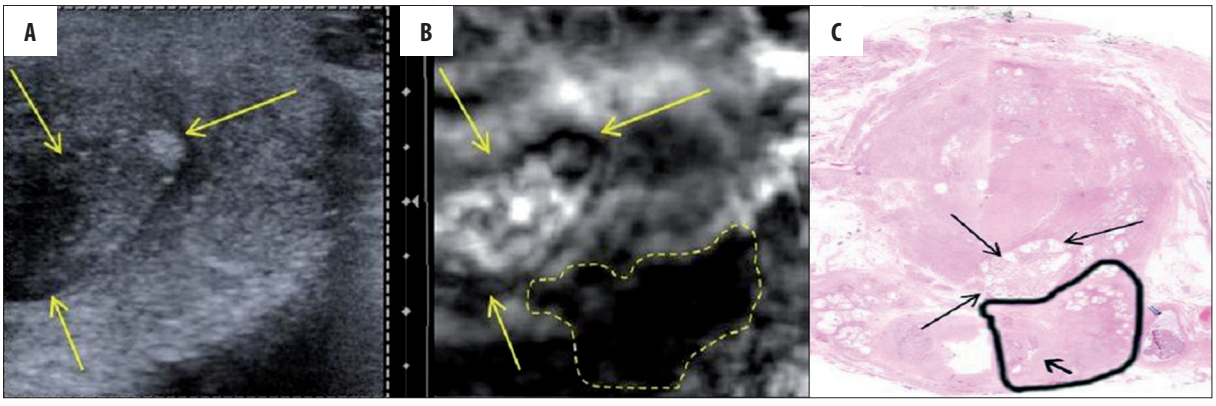

Figure 5. Axial section of prostate specimen #1 peripheral zone. Left lateral section of the prostate's base; classic ultrasound B-mode (**A**) and elastogram (**B**). Hard lesion is outlined, arrows point to adjacent nodule. (**C**) Hematoxylin & eosin stained histological section of prostate base. The tumor (Gleason score 3+5=8, outlined in black) extended beyond the prostatic capsule in this section and invaded the left seminal vesicle (arrow).

Table 1. Table summarizing the experimental results of the palpation study: sensitivity and specificity.

	Manual palpation	Ultrasound elastography
Sensitivity	66%	84%
Specificity	67%	71%
Detection rate <20 mm depth	80%	68%
Detection rate >20 mm depth	0%	66%
Detection rate	80%	84%

ultrasound research interface to access raw RF data. Data was acquired by manual handling using a Siemens VF 10-5 linear array for prostate specimens. After RF data collection, elastograms were obtained using the dynamic programming (DP) elastography algorithm developed in our lab [27,28].

Each prostate specimen underwent routine pathologic processing and analysis. Due to the high volume of prostatectomies performed at our institution, the routine pathological process does not result in a whole mount mapping. Instead, for histopathological evaluation the prostatectomy specimens were initially sliced at every 3–4 mm from apex to base, according to the Stanford protocol. Each slice (6 to 10 master slices) were then incorporated in a paraffin block and sliced at 5 µ meter thickness. The slices were stained with hematoxylin-eosin and were then analyzed under a microscope by a pathologist blinded to the surgeon's findings and also to the elastography results. The localization and size of each tumor focus were documented for all step master slices on axial diagrams, with Gleason score. Large macro photographs were reconstructed in several specimens (Figure 5C). All data collected were stored in the database.

N=10 target areas were analyzed from N=6 patients enrolled so far into the elastography analysis. Histological findings served as the *gold standard* in determining the presence, location and size of any prostatic nodules, malignant and benign. The objective of our study was then to compare axial elastograms findings with the histological findings recorded by the pathologist (mapping diagrams, measurements and nodule characteristics such as malignant *vs.* benign). Since histopathology diagrams often specified just the maximum diameter of a lesion, coronal elastograms were used to better establish the location and extent of the identified lesions. MRI images (both axial and coronal planes) were aligned to the elastograms and provided help with their anatomical co-registration using anatomical details such as urethra or boundaries of peripheral zone *vs.* central gland.

Results

Comparative study for tumor detection

Overall sensitivity and specificity results are summarized in Table 1. USE showed higher accuracy in tumor detection with a sensitivity of 84% and specificity of 71%, compared to a sensitivity of 66% and a specificity of 67% for manual palpation. At depths greater than 20 mm, no subject was able to identify a lesion by manual palpation. 66% of these lesions were correctly identified on elastograms.

Diameter estimation for synthetic phantoms using manual palpation was less accurate than USE (p=0.001) with a root mean squared error of estimation (RMSE) of 4.81 for manual palpation (95% CI between 3.83 and 5.78), versus mean RMSE=3.02 for USE (95% CI between 2.57 and 3.47). For *ex-vivo* phantoms, estimations were comparable in both manual palpation and USE, at a RMSE of about 11.0 mm. Depth estimation for synthetic phantoms was statistically higher using manual palpation than USE (p=0.0001) with a mean value of the RMSE of 8.81 for manual palpation (95% CI between 6.24 and 11.39) versus a mean value of the RMSE=3.02 for USE (95% CI between 2.42 and 3.63) – Figure 3. For *ex-vivo* phantoms, estimations were comparable again for both manual palpation and USE, at a RMSE of about 1.0 mm.

Ex-vivo human prostate study

Elastography identified N=10 lesions, 8 hard nodules in the peripheral zone, 1 hard and 1 soft nodule in the central gland (Table 2). Pathology reports showed 8 of these

Table 2. Prostate specimen data: A total of 10 (ten) elastography lesions were identified in 6 (six) patients' specimens (8 malignant and 2 benign).

#	Location	Gleason score	Size (cm)		
			Elastography	Pathology	MRI
1.1	PZ base	3+5	1.4×0.8	1.3×0.8	1.3×1.1
1.2	CG base	N/A-Solid	0.7×1.1	1.0×1.0	1.0×1.1
1.3	CG base	N/A-Soft	1.1×0.8	1.0×1.0	1.0×0.9
2.1	PZ base	5+3	3.0×1.3	2.4×1.0	2.0×1.5
3.1	PZ mid	4+5	2.4×0.8	1.9×1.0	1.5×1.2
4.1	PZ mid	3+3	1.0×0.5	0.5×0.4	0.6×0.7
4.2	PZ mid	3+4	1.5×0.9	1.1×0.5	1.1×0.8
5.1	PZ apex	3+3	0.5×0.6	0.5×0.5	0.6×0.6
5.2	PZ apex	4+3	0.6×1.0	0.8×0.9	0.9×0.9
6.1	PZ base	3+3	0.7×1.2	0.7×1.8	0.7×0.7

PZ – peripheral zone; CG – central gland.

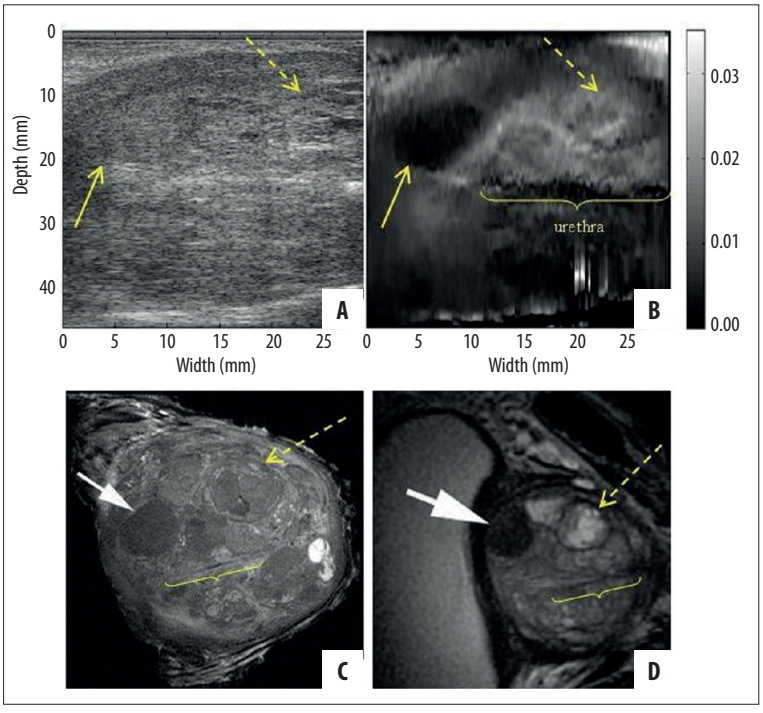

Figure 6. Coronal section of prostate specimen #1 at the level of the central gland. Classic ultrasound B-mode (**A**) and elastogram (**B**). 9.4 Tesla *ex-vivo* (**C**) and 3 Tesla *in-vivo* (**D**) MRI images are presented in coronal planes, in CCW (counter clock wise) orientation for better visualization of the correlation between USE and MRI of the specimen. Benign solid (arrow) and soft (dashed arrow) nodules and urethra are visible.

lesions as malignant and 2 as benign. Diameter measurements correlation proved difficult because of the inability to perfectly register the three investigative modalities. USE and MRI measurements were within on average 2.05 mm *vs.* 2.25 mm of the diameters measured by pathology (standard deviation of 1.9 mm for USE and 2.9 mm for MRI). Size measurements and Gleason score are reported in Table 2.

Specimen #1 presented multiple hard and soft lesions, located in the central gland of the prostate (Figure 6). The *ex-vivo* T2-weighted coronal image from specimen MRI obtained at 9.4 Tesla (Figure 6C) – here in counter clock wise orientation for better visualization of the correlation between USE and MRI of the specimen) shows detailed anatomy of the heterogeneous central gland with a solid benign prostatic hypertrophy nodule (BPH) confirmed by pathology. Elastography was able to detect this solid nodule despite the heterogeneity of the prostate (Figure 6B) – solid arrow, whereas the lesion was not clearly identified by gray scale ultrasound. *Ex-vivo* T2-weighted 9.4 Tesla coronal image from specimen MRI also shows an additional soft cystic BPH nodule (dashed arrow). Urethra is also visible on the elastogram, as well as MRI exam (labeled *urethra*).

Axial scans of the same specimens were compared with histopathology axial cross-sections. The prostate, submitted for

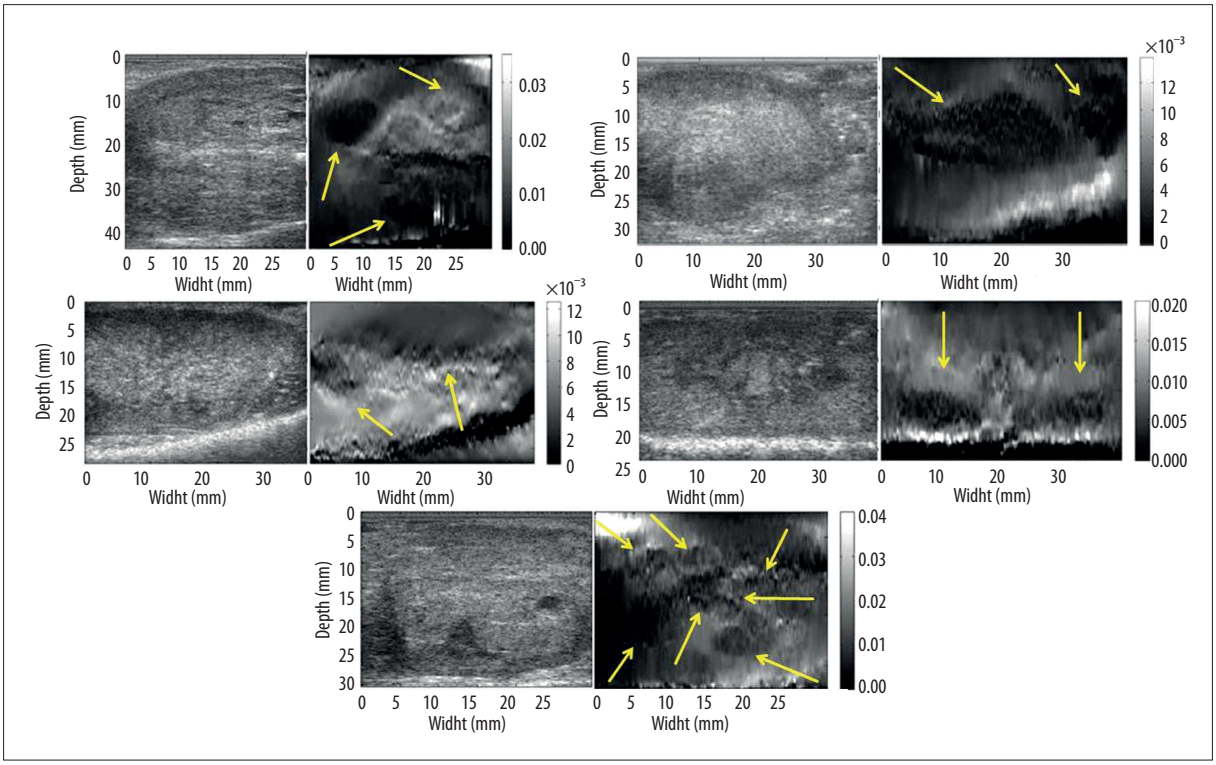

Figure 7. B-mode image (left) and elastogram (right) from specimens # 2–6. Dark regions at the very bottom of elastograms represent structures outside the prostate tissue (e.g. operating table). The border of the prostatic tissue can be easily noticed as a highly reflective band at the bottom of B-mode images.

histological processing in four quadrant sections per slice, was digitally realigned to reconstruct a full histological cross-section (Figure 5C). Specimen #1 was found with a tumor with Gleason score of 8 at the prostate base, left side (outlined). Figure 5A shows an ultrasound B-mode image and an elastogram obtained through an axial plane at the prostate's base on the left side. The same tumor was identified by elastography (Figure 5B – dashed contour) but is not visible on grey-scale ultrasound. For an anatomical correlation, a soft - cystic nodule anterior to cancer can be seen on B-mode image and USE (Figure 5A,B – arrows) and on histopathology (Figure 5C – arrows).

The remaining 5 (five) prostate specimens presented with superficial lesions in the peripheral zone of the gland. USE identified multiple hard malignant lesions in various locations, from the base to the apex of the prostate gland. One can notice the clear delimitations of these lesions on USE (Figure 7) as well as the close estimations of size versus pathology and MRI.

Discussion

In surgical procedures where manual palpation would be helpful but not possible to perform, e. g. laparoscopic robotic surgery, USE can offer added value if proven to be accurate in detecting pathologic lesions. Our comparative study showed USE to be superior to manual palpation in general sensitivity and specificity, and also in identifying deeper lesions. Despite of the inexperience of our subjects with USE and elastogram evaluation, USE demonstrated good performance in detection of hard lesions. This is particularly important as surgeons can be considered inexperienced elastogram readers as well. Our feasibility study showed that USE was able to identify both hard and soft lesions in the *ex-vivo* prostate specimens, located in the deep prostatic central gland and in the peripheral zone. Histopathologic findings validated USE, and results compared favorably with the *in-vivo* pre-surgical and *ex-vivo* post-surgical MRI scans. In the central gland of the prostate, elastography showed excellent detection of hard and soft areas, despite the complexity of the central gland. Elastography was able to identify both hard and soft BPH nodules and anatomical landmarks like the urethra (note excellent anatomical correlation to MR scan findings). In the peripheral zone USE identified multiple hard malignant lesions, from the base to the apex of the prostate gland. These preliminary results demonstrate the ability of USE to detect hard nodules in the prostate and are encouraging in the pursuit of this technology as a palpation equivalent imaging tool for prostatectomy.

USE maps tissue elasticity which makes it an ideal imaging modality to serve as a surrogate and possible equivalence to manual palpation in identifying hard cancerous tissue in the prostate gland, especially in the peripheral zone but also in the central gland. Real-time intra-operative imaging guidance is needed for identifying the presence of cancer within the prostate, especially near the capsule where tumor can invade and spread outside of the gland, and also for studying surrounding structures. If diseased hard lymph nodes could be detected, then lymphadenectomy may provide a more accurate cancer staging, help tailor future therapy, and potentially prevent recurrence. A better delineation of the bladder neck and apex during dissection, especially

when prostate cancer is located at the apex could perhaps improve patients' outcome. If deemed possible, imaging cavernous nerves (CNs) located along the immediate surface of the prostate gland may lead to their preservation, and thus improved preservation of potency and urinary continence [29]. Further more, the development of the elastography technology as an imaging guiding tool during prostatectomy could potentially be useful in the open procedures as well, where the manual palpation would not be enough to identify deeper lesions. It has been documented in the literature that prostate carcinoma originates in the central gland and transitional zone in up to 30% of cases [30,31].

Conclusions

Our initial experience showed USE was able to reliably identify hard nodules in the peripheral zone of the prostate that were prostate cancers. Additionally, USE showed its ability to define tissue hardness of BPH nodules despite the underlying tissue complexity in the central gland. Our comparative study demonstrated USE can approach the efficacy of manual palpation for superficial lesions and has the potential to surpass it for smaller, deeper lesions. We employed a laparoscopic ultrasound probe which was successfully used and tested in conjunction with elastography algorithms. Our initial experience with USE encourages us to pursue further the evaluation of this technique. Further testing of the laparoscopic probe is needed in a real laparoscopic environment. We can conclude that there is promise is integrating laparoscopic ultrasound elastography as a real-time, *in-vivo* imaging tool to guide surgeons during robotic-assisted prostatectomies.

Acknowledgements

We thank our colleagues, surgeon Mohammed Allaf and Naima Carter-Monroe, and also Intuitive Surgical for their help. Ioana Fleming is supported by the Department of Defense Prostate Cancer Predoctoral Fellowship.

References:

1. Jemal A, Siegel R, Xu J, Ward E: Cancer statistics, 2010. CA: A Cancer Journal for Clinicians. 2010; 60(5): 277–300
2. Bill-Axelson A, Holmberg L, Ruutu M et al: Radical prostatectomy versus watchful waiting in early prostate cancer. N Engl J Med, 2011; 364(18): 1708–17
3. Box GN, Ahlering TE: Robotic radical prostatectomy: long-term outcomes. Curr Opin Urol, 2008; 18(2): 173–79
4. Pruthi RS, Wallen EM: Current status of robotic prostatectomy: promises fulfilled. J Urol, 2009; 181(6): 2420–21
5. Nelson B, Kaufman M, Broughton G et al: Comparison of length of hospital stay between radical retropubic prostatectomy and robotic assisted laparoscopic prostatectomy. J Urol, 2007; 177(3): 929–31
6. Artibani W, Fracalanza S, Cavalleri S et al: Learning curve and preliminary experience with da Vinci-assisted laparoscopic radical prostatectomy. Urol Int, 2008; 80(3): 237–44
7. Colombo J, Jose R, Santos B et al: Robotic assisted radical prostatectomy: surgical techniques and outcomes. International Braz J Urol, 2007; 33(6): 803–9
8]. Badani KK, Kaul S, Menon M: Evolution of robotic radical prostatectomy: assessment after 2766 procedures. Cancer, 2007; 110(9): 1951–58
9. Ficarra V, Cavalleri S, Novara G et al: Evidence from robot-assisted laparoscopic radical prostatectomy: a systematic review. Eur Urol, 2007; 51(1): 45–55; discussion 56
10. Berryhill J Roy, Jhaveri J, Yadav R et al: Robotic prostatectomy: a review of outcomes compared with laparoscopic and open approaches. Urology, 2008; 72(1): 15–23
11. Hu JC, Wang Q, Pashos CL et al: Utilization and outcomes of minimally invasive radical prostatectomy. J Clin Oncol, 2008; 26(14): 2278–84
12. Walsh PC, Lepor H, Eggleston JC: Radical prostatectomy with preservation of sexual function: anatomical and pathological considerations. Prostate, 1983; 4(5): 473–85
13. Salomon G, Kllerman J, Thederan I et al: Evaluation of prostate cancer detection with ultrasound real-time elastography: a comparison with step section pathological analysis after radical prostatectomy. Eur Urol, 2008; 54(6): 1354–62
14. Ukimura O, Gill IS, Desai MM et al: Real-time transrectal ultrasonography during laparoscopic radical prostatectomy. J Urol, 2004; 172(1): 112–18
15. Ukimura O, Magi-Galluzzi C, Gill IS: Real-time transrectal ultrasound guidance during laparoscopic radical prostatectomy: impact on surgical margins. J Urol, 2006; 175(4): 1304–10
16. Coley CM, Barry MJ, Fleming C, Mulley AG: Early detection of prostate cancer. Part I: Prior probability and effectiveness of tests. Ann Intern Med, 1997; 126(5): 394–406
17. Daehnert WF, Hamper UM, Eggleston JC et al: Prostatic evaluation by transrectal sonography with histopathologic correlation: the echopenic appearance of early carcinoma. Radiology, 1986; 158(1): 97–102
18. Ophir J, Alam SK, Garra B et al: Elastography: ultrasonic estimation and imaging of the elastic properties of tissues. Proc Inst Mech Eng H, 1999; 213(3): 203–33
19. Cochlin DL, Ganatra RH, Griffiths DFR: Elastography in the detection of prostatic cancer. Clin Radiol, 2002; 57(11): 1014–20
20. Koenig K, Scheipers U, Pesavento A et al: Initial experiences with real-time elastography guided biopsies of the prostate. J Urol. 2005; 174(1): 115–17
21. Sumura M, Shigeno K, Hyuga T et al: Initial evaluation of prostate cancer with real-time elastography based on step-section pathologic analysis after radical prostatectomy: a preliminary study. Int J Urol, 2007; 14(9): 811–16
22. Leven J, Burschka D, Kumar R et al: DaVinci canvas: a telerobotic surgical system with integrated, robot-assisted, laparoscopic ultrasound capability. Med Image Comput Comput Assist Interv, 2005; 8(Pt 1): 811–18
23. Schneider CM, Dachs GW II, Hasser CJ et al: Robot-assisted laparoscopic ultrasound. In: Proceedings of the First international conference on Information processing in computer-assisted interventions. IPCAI'10. Berlin, Heidelberg: Springer-Verlag, 2010; 67–80
24. Schneider CM, Peng PD, Taylor RH et al: Robot-assisted laparoscopic ultrasonography for hepatic surgery. Surgery, 2012; 151(5): 756–62
25. Billings S, Deshmukh N, Kang HJ et al: System for robot-assisted real-time laparoscopic ultrasound elastography. In: Proceedings of the SPIE Medical Imaging, 2012; 67
26. Mansy HA, Grahe JR, Sandler RH: Elastic properties of synthetic materials for soft tissue modeling. Phys Med Biol, 2008; 53(8): 2115–30
27. Rivaz H, Boctor E, Foroughi P et al: Ultrasound elastography: a dynamic programming approach. IEEE Trans Med Imaging, 2008; 27(10): 1373–77
28. Rivaz H, Boctor EM, Choti MA, Hager GD: Real-time regularized ultrasound elastography. IEEE Trans Med Imaging, 2011; 30(4): 928–45
29. Su L, Link RE, Bhayani SB et al: Nerve-sparing laparoscopic radical prostatectomy: replicating the open surgical technique. Urology, 2004; 64(1): 123–27
30. McNeal JE, Redwine EA, Freiha FS, Stamey TA: Zonal distribution of prostatic adenocarcinoma. Correlation with histologic pattern and direction of spread. Am J Surg Pathol, 1988; 12(12): 897–906
31. Cohen RJ, Shannon BA, Phillips M et al: Central zone carcinoma of the prostate gland: a distinct tumor type with poor prognostic features. J Urol, 2008; 179(5): 1762–67; discussion 1767